Localized surfaces of three-dimensional topological insulators

Yang-Zhi Chou, Rahul M. Nandkishore, and Leo Radzihovsky

Phys. Rev. B **99**, 165108 — Published 8 April 2019

DOI: 10.1103/PhysRevB.99.165108

Localized surfaces of three dimensional topological insulators

Yang-Zhi Chou,* Rahul M. Nandkishore, and Leo Radzihovsky
Department of Physics and Center for Theory of Quantum Matter, University of Colorado Boulder, Boulder, Colorado 80309, USA
(Dated: March 20, 2019)

We study the surface of a three-dimensional spin chiral Z_2 topological insulator (class CII), demonstrating the possibility of its localization. This arises through an interplay of interaction and statistically-symmetric disorder, that confines the gapless fermionic degrees of freedom to a network of one-dimensional *helical* domain-walls that can be localized. We identify two distinct regimes of this gapless insulating phase, a "clogged" regime wherein the network localization is induced by its junctions between otherwise metallic helical domain-walls, and a "fully localized" regime of localized domain-walls. The experimental signatures of these regimes are also discussed.

I. INTRODUCTION

The surfaces of topological insulators (TIs)[1–4] exhibit robust symmetry-protected metallic transport even in the presence of symmetry-preserving heterogeneity (disorder) as long as the bulk remains gapped. The evasion of Anderson localization[5,6] is due the anomalous nature of the surface states, reflecting a nontrivial wavefunction topology of TI's bulk. Characterization of such symmetry protected topological materials is a vibrant field of research in modern condensed matter physics[7,8].

Interactions can destabilize such metallic surfaces[9–13] gapping them out by either spontaneously breaking the protective symmetry, or inducing a symmetry-preserving topologically-ordered long-range entanglement. However, it has been noted[14,15] and explored more extensively by us[16], that in a two-dimensional (2D) time-reversal symmetric Z_2 TI (class AII)[17–19] an interplay of interaction and disorder can lead to another possibility, namely to a glassy gapless but *insulating* edge. Such a localized state breaks the time-reversal symmetry spontaneously, but in "spin glass" fashion, preserving it statistically. It exhibits a localization length that is a non-monotonic function of disorder strength, and is best viewed as localized insulator of half charge fermionic domain-walls (Luther-Emery[20] fermons)[16]. Such edge localization provides a potential explanation of the puzzling experimental observations in InAs/GaSb TI systems[21–24].

Motivated by this nontrivial disorder-interaction interplay in an edge of a 2D TI, we explore such phenomena in a 2D surface of a three-dimensional (3D) TI and find that only the CII class realizes this idea, namely, exhibits a *gapless localized* surface. We thus focus on the CII class TIs in the presence of symmetry breaking, but statistically preserving disorder. Such a disorder potential can in principle be generated dynamically[26,27]. It allows for three distinct possibilities: a network of chiral (particle-hole symmetric) or helical (time-reversal symmetric) domain-walls[28] (see Fig. 1), or a fully gapped (time-reversal and particle-hole symmetry-broken) insulators, depending on which symmetries are broken by disorder. As we demonstrate below, for the second case of a network of helical domain-walls, in the presence of interactions, a CII class TI surface indeed displays a phase transition to a *gapless insulating* surface. The latter exhibits two regimes: a "clogged" regime in which the barriers to transport are the junctions in the network of otherwise delocalized domain-walls[29], and a fully localized regime of interpenetrating 1D localized helical edge states[16]. These interaction-induced regimes are obtained via standard analysis for helical Luttinger liquids[14–16,29]. Topological insulators in other symmetry classes of the ten-fold way do not allow this novel possibility.

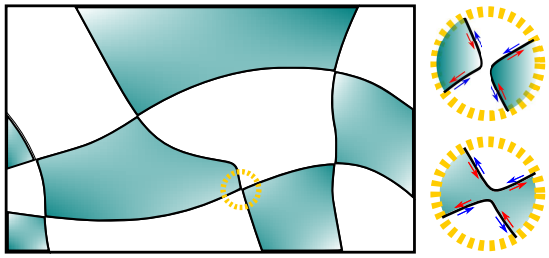

FIG. 1. An illustration of a disordered interacting class CII TI surface, forming helical domain-walls (black solid curves), between topologically gapped green domains[25] and trivially gapped white regions. Zoom-in: The interdomain four-way junction modeled as two helical Luttinger liquids with an impurity (junction) perturbation.

The article is organized as follows. We begin in Sec. II with an introduction of a continuum model of a surface of CII class TI. We discuss three classes of symmetry-breaking heterogeneities that preserve its statistical symmetry in Sec. III, focusing on the helical network surface. A single interacting helical junction is studied in Sec. IV B, and is utilized to make arguments for a localization transition in the helical surface network. We conclude with experimental signatures and the future directions in Sec. V.

II. SURFACE MODEL

Three dimensional TIs are characterized by symmetry-protected metallic surfaces that host 2D massless Dirac or Majorana quasiparticles[1,2,30]. In the absence of inter-

action, they are robust to gapping out or localization by any symmetry-preserving single particle scattering. We focus on the spin chiral TI (class CII)[30,31], characterized by a Z_2 invariant. Its topologically nontrivial surface exhibits two-valley Dirac cones with the chemical potential pinned to the Dirac point. The corresponding noninteracting clean CII surface Hamiltonian is given by

$$H_0 = v_D \int_{\mathbf{x}} \Psi^\dagger \left[-i\hat{\sigma}^x \partial_x - i\hat{\sigma}^y \partial_y\right] \Psi, \tag{1}$$

where Ψ is a four component fermionic Dirac field and $\hat{\sigma}^{x,y,z}$ is the "spin" Pauli matrix.

The clean surface Hamiltonian, H_0 can be perturbed by a number of fermion bilinear operators, $\Psi^\dagger \hat{T}_a \Psi$ (listed in Table I), that can be classified by their commutation/anticommutation with $\hat{\sigma}^x$ and $\hat{\sigma}^y$ ($[\hat{T}_a, \hat{\sigma}^x]$, $[\hat{T}_a, \hat{\sigma}^y]$, $\{\hat{T}_a, \hat{\sigma}^x\}$, and $\{\hat{T}_a, \hat{\sigma}^y\}$). If a bilinear commutes with both the $\hat{\sigma}^x$ and $\hat{\sigma}^y$, it is regarded as a scalar operator, denoted by $\hat{V}_a$. A vector operator, $\hat{A}_a$, commutes with one of the $\hat{\sigma}^x$ or $\hat{\sigma}^y$, but anticommutes with the other one. The mass operator, $\hat{M}_a$, anticommutes with both the $\hat{\sigma}^x$ and $\hat{\sigma}^y$.

We first focus on the symmetric bilinear operators given by

$$H_{\rm dis} = \int_{\mathbf{x}} \Psi^\dagger \left[v_1 \hat{\tau}^x + v_2 \hat{\tau}^z + a_1 \hat{\sigma}^x \hat{\tau}^y + a_2 \hat{\sigma}^y \hat{\tau}^y\right] \Psi, \tag{2}$$

where $\hat{\tau}^{x,y,z}$ is the "valley" Pauli matrix. The bilinear operators $v_1(\mathbf{x})$, $v_2(\mathbf{x})$ are scalar and $a_1(\mathbf{x})$, $a_2(\mathbf{x})$ vector, time- and particle-hole symmetry-preserving random potentials? . The time reversal ($\mathcal{T}$) and the particle-hole ($\mathcal{P}$) operations are defined by

$$\mathcal{T} : \Psi \to i\hat{\sigma}^y \Psi, \;\; i \to -i, \tag{3a}$$

$$\mathcal{P} : \Psi \to \hat{\sigma}^x \hat{\tau}^y (\Psi^\dagger)^T. \tag{3b}$$

We note that the matrices in both symmetry operations ($\hat{\sigma}^y$ and $\hat{\sigma}^x\hat{\tau}^y$) are antisymmetric because they correspond to $\mathcal{T}^2 = -1$ and $\mathcal{P}^2 = -1$[3,4]. In addition, a chiral operation ($\mathcal{S} = \mathcal{T}\mathcal{P}$) can be defined as a product of $\mathcal{T}$ and $\mathcal{P}$. All the bilinear operators in Table I are classified by these symmetries as well.

We now consider symmetry-breaking random bilinear perturbations to the $\mathcal{T}$, $\mathcal{P}$ symmetric CII surfaces. Although (as listed in Table I) there are various scalar ($\hat{V}_a$) and vector ($\hat{A}_a$) operators, these do not open up a gap or induce a localization, unlike the mass operator $\hat{M}_a$[25,33]. We thus focus on random symmetry-breaking masses, $H_{\rm M} = \sum_{a=1}^4 H_{{\rm M},a}$, with

$$H_{{\rm M},a} = \int_{\mathbf{x}} m_a(\mathbf{x}) \Psi^\dagger \hat{M}_a \Psi. \tag{4}$$

These can be classified as follows (also in Table I): $\hat{M}_1 = \hat{\sigma}^z$ preserves $\mathcal{P}$ but breaks $\mathcal{T}$; $\hat{M}_2 = \hat{\sigma}^z\hat{\tau}^y$ preserves $\mathcal{T}$ but breaks $\mathcal{P}$; $\hat{M}_3 = \hat{\sigma}^z\hat{\tau}^x$ and $\hat{M}_4 = \hat{\sigma}^z\hat{\tau}^z$ preserve $\mathcal{S} = \mathcal{T}\mathcal{P}$ but break both $\mathcal{T}$ and $\mathcal{P}$.

$\hat{T}_a$	Billinear operator	$\mathcal{T}$	$\mathcal{P}$	$\mathcal{S}$	Class
$\hat{V}_{1,2}$	$\hat{\tau}^x$, $\hat{\tau}^z$	✓	✓	✓	CII
$\hat{A}_{1,2}$	$\hat{\sigma}^x\hat{\tau}^y$, $\hat{\sigma}^y\hat{\tau}^y$	✓	✓	✓	CII
$\hat{V}_3$	$\hat{\tau}^y$	×	✓	×	C
$\hat{A}_{3,4,5,6}$	$\hat{\sigma}^x\hat{\tau}^x$, $\hat{\sigma}^x\hat{\tau}^z$, $\hat{\sigma}^y\hat{\tau}^x$, $\hat{\sigma}^y\hat{\tau}^z$	×	✓	×	C
$\hat{M}_1$	$\hat{\sigma}^z$	×	✓	×	C
$\hat{V}_4$	$\hat{1}$	✓	×	×	AII
$\hat{M}_2$	$\hat{\sigma}^z\hat{\tau}^y$	✓	×	×	AII
$\hat{A}_{7,8}$	$\hat{\sigma}^x$, $\hat{\sigma}^y$	×	×	✓	AIII
$\hat{M}_{3,4}$	$\hat{\sigma}^z\hat{\tau}^x$, $\hat{\sigma}^z\hat{\tau}^z$	×	×	✓	AIII

TABLE I. Classification of the bilinear operators in terms of the time-reversal ($\mathcal{T}$), particle-hole ($\mathcal{P}$), and chiral ($\mathcal{S} = \mathcal{T}\mathcal{P}$) operations on the CII class [as defined in Eq. (3)], and the type of perturbations ($\hat{V}_a$, $\hat{A}_a$, and $\hat{M}_a$).

For our purposes here, we imagine simply imposing the random sign-changing amplitudes, $m_a(\mathbf{x})$, such that statistically (averaged over disorder or samples) $\mathcal{T}, \mathcal{P}$ symmetries remain intact, i.e., m_a has zero mean. More physically, such random mass operators can arise as a result of heterogeneous spontaneous symmetry breaking in the presence of symmetric quenched disorder $H_{\rm dis}$ and four-Fermi interactions

$$H_I = \sum_{a=1}^4 U_a \int_{\mathbf{x}} \left[\Psi^\dagger \hat{M}_a \Psi\right]^2, \tag{5}$$

where U_a denotes the interaction strength corresponding to the mass $\hat{M}_a$[26,27], with $m_a(\mathbf{x})$ the mean-field order parameter determined self-consistently[26].

Independent of the physical mechanism, we expect the CII symmetry-breaking random perturbation $H_{\rm M}$ to generate a surface ground state that is a network of 1D domain walls, similar to statistical topological insulators[25,34], illustrated in Fig. 1, the fate of which, in the presence of interactions is the focus of our work.

III. CII CLASS SYMMETRY-BROKEN SURFACE STATES

In a three-dimensional CII class TI, the random symmetry-breaking mass operators $\hat{M}_a$ can lead to three types of domain-wall networks, corresponding to three distinct symmetries of sign-changing masses $m_a(\mathbf{x})$ introduced in Sec. II (see Table I). As we will discuss below, with one type of a mass, the inhomogeneous symmetry breaking leads to a surface state composed of a network of gapless 1D domain-walls separating domains characterized by a positive and negative value of a mass m_a. In the CII class, it is also possible to generate multiple mass terms when only the chiral symmetry ($\mathcal{S}$) is preserved. In this case the symmetry-breaking order parameter is a

vector, that can rotate smoothly without vanishing, and as a result, such surface state, previously discussed[9–13], is fully gapped. Looking for a new, gapless but localized TI surface scenario, here we instead focus on the case only time-reversal ($\mathcal{T}$) or particle-hole ($\mathcal{P}$) symmetry is unbroken, such that there are sharp gapless domain-walls, that we will argue can get localized for the case of $\hat{M}_2$ disorder in the presence of interactions.

The transport in such symmetry-broken surface states of CII TIs is governed by the resulting network of the massless 1D domain-walls. The domain-wall surface states can be derived analytically in the large domain size limit via the standard "twist mass" formalism[35,36]. The 1D nature of the domain-walls is interrupted by regions where two domain walls come close to each other. These can be modeled as junctions illustrated in Fig. 1.

Here we are outlining the underlying physics and the approach, relegating the technical analysis to the Appendices. To make progress, we take the effect due to the random mass symmetry-breaking operators [given by Eq. (4)] to be much stronger than the symmetric disorder [given by $H_{\rm dis}$ in Eq. (1)]. Therefore, we first compute the zero energy states of $H_0 + H_{{\rm M},a}$, determining the structure of the 1D electron domain-walls. We find that only one class, the helical domain-walls, arising by domains breaking $\mathcal{P}$ but not $\mathcal{T}$ symmetry, have the possibility of localization. We then study the stability of the resulting network to interactions and symmetric disorder, $H_{\rm dis}$, taking advantage of our earlier work on 1D edges of 2D TIs[16], as well as the analysis of the four-way junctions[29]. The other symmetry-breaking scenarios are robust to symmetric disorder and interactions and thus such disordered TI surfaces remain metallic.

A. Particle-hole symmetric surface: Chiral domain-wall network

A particle-hole symmetric but time-reversal broken surface corresponds to the random mass operator $\hat{M}_1 = \hat{\sigma}^z$. In this case the 1D domain-walls are chiral with two co-moving electrons. The chiral domain-wall states can be viewed as the spin quantum Hall edge of class C[37–40]. The intersections or proximity of chiral domain-walls can only rearrange their connectivity, but cannot stop the network state from conducting. Such a metallic state can be realized as a statistical topological insulator[25,34], or, alternatively can be viewed as a critical state at the plateau transition[6]. These are well known to be robust against local symmetric disorder perturbations, as with conventional quantum Hall states. We are not aware of any new physics to be discovered here from the interplay of disorder and interactions, at least in the large domain size limit, where the domain-wall structure can be derived analytically.

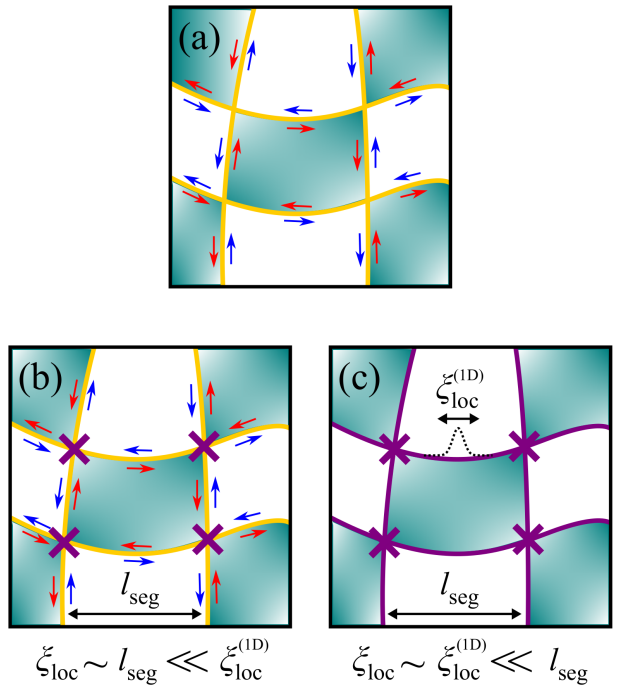

FIG. 2. Three possible regimes in the helical domain-wall networks. (a) Metallic regime. The helical network remains conducting for weaker Luttinger liquid interaction, $K > 1/2$. (b) "Clogged" regime. For $3/8 < K \leq 1/2$, the symmetric disorder remains irrelevant, but the random junctions (intersections) of the helical domain-walls are relevant and therefore block the dc transport, with helical electrons confined in the inter-junction domain-wall segments, breaking time-reversal symmetry spontaneously[29]. A clogged state also persists for $K < 3/8$ when the 1D domain-wall localization length ($\xi_{\rm loc}^{(1D)}$) is much longer than the typical length of the domain-wall segment ($l_{\rm seg}$). As indicated in the figure, in the clogged regime, the true physical localization length, $\xi_{\rm loc}$ is set by $l_{\rm seg}$. (c) "Fully-localized" regime. For $K \leq 3/8$ and sufficiently small 1D domain-wall localization length ($\xi_{\rm loc}^{(1D)} \ll l_{\rm seg}$), the whole domain-wall network becomes localized with a localization length set by $\xi_{\rm loc}^{(1D)}$. The yellow (purple) solid lines indicate the conducting (localized) channels; the purple crosses mark the perfect barrier junctions; the blue and red arrows indicate the movement of the domain-wall electrons that form Kramers pairs in each domain-wall segment.

B. Time-reversal symmetric surface: Helical domain-wall network

We now turn to the most interesting case with a time-reversal symmetric surface, but with particle-hole symmetry randomly broken by the mass operator $\hat{M}_2 = \hat{\sigma}^z\hat{\tau}^y$. In this case, the domain-walls form a helical network state[28], protected against localization in the absence of interactions[17,41], and have been studied previously[42–45]. We emphasize that class CII TI is the only ten-fold way insulator that realizes a network of helical states under inhomogeneous symmetry breaking. The surface remains metallic as long as the time-reversal sym-

metry is intact. We next discuss the stability of this metallic helical network to interactions and symmetry-preserving disorder in the remainder of this subsection, with the technical analysis presented in Sec. IV B.

Such surface transport is governed by the network of interacting helical domain-walls. At length scales shorter than the distance between junctions the physics is controlled by isolated helical domain walls, analyzable as a helical Luttinger liquid[14,15]. For sufficiently strong repulsive interactions, $K < 3/8$, these can be localized[14–16] due to an interplay of symmetric disorder and umklapp four-fermion interaction[16]. Such a localized state spontaneously and inhomogeneously breaks the time-reversal symmetry and is best viewed by a localized insulator of $e/2$-charge Luther-Emery fermions[16]. Thus for $K < 3/8$, such TI surface becomes a network of localized one-dimensional insulators. This picture is self-consistent as long as the localization length along the one-dimensional domain-walls is short compared to the typical distance between junctions of the network, a condition that can be satisfied by taking the domains to be sufficiently large.

In the complementary regime of weaker interactions, $K > 3/8$, the isolated 1D domain-wall segments are *not* localized, requiring an analysis of the full network, controlled by domain-walls proximity (intersections), that we model as four-way junctions. The latter problem is related to the earlier studies of the corner junction[46] and the point contact[29]. We perform a complementary analysis based on two helical Luttinger liquids with symmetry-allowed impurity perturbations in Sec. IV B and Appendix B. As we will demonstrate, for sufficiently strong interactions, $K < 1/2$, the junctions become strong impurity barriers that suppress all conduction (before, i.e., for weaker interaction than localization of isolated domain-walls, $K < 3/8$[14–16]), and break the time-reversal symmetry spontaneously. Our results are consistent with the earlier finding in the helical liquid point contact study with spin-orbit couplings[29].

Combining the results from both the junction and the domain-wall states, we conclude the existence of three regimes (summarized in Fig. 2) in the large domains limit. For weak interactions ($K > 1/2$), the helical network remains conducting and can be viewed as a statistical TI surface[25,34]. For intermediate interactions ($3/8 < K \leq 1/2$), the junctions break time-reversal symmetry spontaneously and suppress the conduction. The domain-wall state in each segment remains "delocalized", but the junctions block transport. We refer to this as a "clogged" regime. For sufficiently strong interactions ($K \leq 3/8$), all the junctions and the domain-wall segments break time-reversal symmetry spontaneously and form a network of localized one-dimensional channels. Because the "clogged" and "fully localized" states are qualitatively the same, they are two distinct regimes connected by a smooth crossover (driven by interaction strength K) within a single insulating phase that sets in for $K < 1/2$. We discuss this crossover further in Sec. IV B.

C. Surface with only chiral symmetry: Gapped insulator

Lastly, for completeness, we discuss the CII TI surface with both time-reversal and particle-hole symmetry broken by two mass operators, $\hat{M}_3 = \hat{\sigma}^z\hat{\tau}^x$ and $\hat{M}_4 = \hat{\sigma}^z\hat{\tau}^z$, corresponding to the chiral symmetric class AIII. Qualitatively distinct from the case of a single mass, such symmetry broken surface state is typically fully gapped because the domains with multiple masses can deform from one to another without closing the gap[25], a possibility that was anticipated in the previous studies[9–13]. Thus, such a surface is a fully gapped insulator up to disorder-induced rare in-gap states.

Finally we note that for a fine-tuned microscopic model, where only one type of bilinear appears, e.g., $\hat{M}_3 = \hat{\sigma}^z\hat{\tau}^x$ or $\hat{M}_4 = \hat{\sigma}^z\hat{\tau}^z$, a domain-wall network can be realized. However, the domain-walls of this network carry conventional one dimensional electrons. They thus do not enjoy the protection of $\mathcal{T}$ symmetry against localization and can therefore be Anderson-localized by disorder alone, in the absence of interactions.

IV. HELICAL DOMAIN-NETWORK ANALYSIS

We now focus on a helical domain-wall network and analyze its stability to interactions and symmetry-preserving disorder. To this end, we first demonstrate localization along independent 1D domain-walls, and then show that the localization is stable to the ever-present domain-wall junctions, whose effect is to enhance localization by shifting the critical point to weaker interactions.

A. Independent helical domain-walls

At short length scales (shorter than the typical inter-junction separation) we can neglect the domain-wall junctions and focus on the nature of individual helical domain-wall segments. In this limit, the problem reduces to independent 1D helical conductors, in the presence of symmetry-preserving disorder and interactions. This problem is technically identical to that of an interacting disordered edge of a 2D TI in the AII class[14–16], that can be localized by the interplay of symmetric disorder and interactions.

To see this, we consider a helical conductor modeled as counter-propagating states of right (R) and left (L) moving helical fermions, with the low-energy disorder-free Hamiltonian given by

$$H_{\rm hLL} = v_F \int_x \left[R^\dagger\left(-i\partial_x R\right) - L^\dagger\left(-i\partial_x L\right)\right] + H_{\rm int}, \quad (6)$$

where v_F is the Fermi velocity and $H_{\rm int}$ encodes the Luttinger liquid interactions[47,48]. Although $H_{\rm hLL}$ takes the

same form as the spinless Luttinger liquid[47,48], it is distinct from it, as in the helical Luttinger liquids the time-reversal symmetry ($R \to L$, $L \to -R$, and $i \to -i$) satisfies $\mathcal{T}^2 = -1$, and thereby forbids single-particle backscattering perturbation, $L^\dagger R$.

Thus symmetric disorder only allows forward scattering,

$$H_{\rm chem} = \int_x V(x) \left(R^\dagger R + L^\dagger L \right), \tag{7}$$

that in the absence of additional interactions does not lead to localization.

The helical Luttinger liquid is also generically stable to the (disorder-free) time-reversal symmetric two-particle umklapp scattering,

$$H_{\rm umklapp} = \int_x \left[e^{i(4k_F - Q)x} : (L^\dagger R)^2 : + \text{h.c.} \right] \tag{8}$$

($: A :$ is the normal ordering of A) as long the reciprocal lattice wavevector Q is sufficiently incommensurate, i.e., as long as $|4k_F - Q| > \delta Q_c$ (δQ_c the critical threshold) is satisfied[49].

However, in the presence of symmetric disorder, that statistically makes up the wavevector incommensuration, the umklapp interaction generates a random time-reversal symmetric two-fermion back-scattering, that can lead to a localization of the 1D helical Luttinger liquid and the associated spin-glass-like time-reversal symmetry breaking[16]. Indeed, the standard renormalization group (RG) analysis shows that an interacting disordered helical conductor can be localized for $K < 3/8$[14,15]. Alternatively, the problem at $K = 1/4$ can be mapped onto noninteracting Luther-Emery fermions[20] with chemical potential disorder[16], a model that is known to give localization for the entire spectrum[50]. Such an interacting localized state is best viewed as an Anderson localized insulator of half-charge fermions (solitons), that exhibits a nonmonotonic localization as a function of disorder strength[16].

Such localization of the 1D helical liquids then directly predicts a localization of long segments of nonintersecting domain-wall, valid in the regime when domain-wall junctions can be neglected. We next analyze the complementary regime where junctions play an essential role in localization of the CII surface.

B. Interacting helical junction

For a weaker electron interaction $K > 3/8$ and/or smaller domain size, the domain-wall intersections become important, and it is necessary to take into account junctions (see zoom-in of Fig. 1). At the technical level, the problem of the four-way helical junction is related to the studies of a corner junction[46] and point contact[29] in a 2D topological insulator. In these previous works, the junction of four semi-infinite helical Luttinger liquids is mapped to an infinite spinful Luttinger liquid with an impurity interaction. We present a technically distinct but physically equivalent analysis based on two isolated Luttinger liquids with junction perturbations.

We thus consider two 1D generic helical Luttinger liquids $+, -$, interacting via a local junction perturbation, corresponding to two helical domain-walls coming to close proximity (see the zoom-in in Fig. 1). Because these are boundaries of the same type of gapped domains, they map onto two 1D Luttinger liquids of opposite helicity, described by two copies of the helical Hamiltonian [Eq. (6)],

$$H_{\rm hLL,2} = v_F \sum_{s=\pm} \int_x \left[R_s^\dagger \left(-i\partial_x R_s \right) - L_s^\dagger \left(-i\partial_x L_s \right) \right] + H_{\rm int,2}, \tag{9}$$

where R_s (L_s) is the right (left) moving fermion, with the index s labeling the two helical domain-walls and $H_{\rm int,2}$ encoding the Luttinger liquid interactions[47] within each helical liquid. For simplicity, we take these two to have the same Fermi velocity (v_F) and Luttinger liquid interaction; we expect our qualitative conclusions to remain valid away from this special case.

To construct junction perturbations, we enumerate all bilinear and quartic operators allowed by the time-reversal symmetry[51,52]. For example, as usual the single-particle backscattering within the same helical liquid ($L_s^\dagger R_s$) is forbidden. We will also ignore perturbations that are always irrelevant in the RG analysis. The single particle forward and backward tunneling processes between the two helical liquids are given by

$$\begin{aligned} H_{\rm junc}^{(1)} = &- t_e \left[L_-^\dagger(0) R_+(0) - R_-^\dagger(0) L_+(0) + \text{H.c.} \right] \\ &- t_{e'} \left[R_-^\dagger(0) R_+(0) + L_-^\dagger(0) L_+(0) + \text{H.c.} \right], \end{aligned} \tag{10}$$

where t_e and $t_{e'}$ are the amplitudes of single electron tunneling. We note that $t_{e'}$ process is only allowed in the presence of Rashba spin-orbit coupling, which breaks the nongeneric spin S_z conservation[29]. For sufficiently strong t_e, the connectivity of the two helical liquids may be restructured. (See the zoom-in of Fig. 1 for the two possible configurations.)

We also include the two-particle "Cooper pair" tunneling processes, given by

$$H_{\rm junc}^{(2)} = -t_{2e} \left[L_-^\dagger(0) R_-^\dagger(0) R_+(0) L_+(0) + \text{H.c.} \right], \tag{11}$$

corresponding to a Kramers pair hopping between two helical domain walls.

Finally, we include the two-particle backscattering across the junction,

$$\begin{aligned} H_{\rm junc}^{(I)} = &- t_\sigma \left[L_+^\dagger(0) R_+(0) L_-^\dagger(0) R_-(0) + \text{H.c.} \right] \\ &- t_{\sigma'} \left[L_+^\dagger(0) R_+(0) R_-^\dagger(0) L_-(0) + \text{H.c.} \right]. \end{aligned} \tag{12}$$

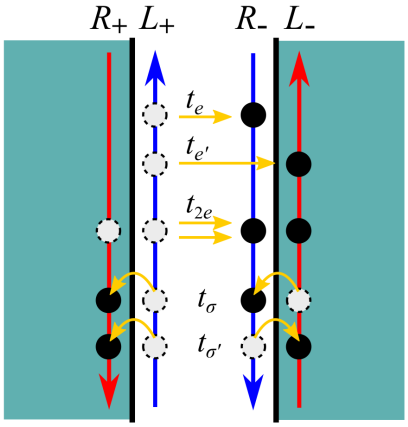

FIG. 3. Illustration of junction perturbations between two helical domain-wall liquids with opposite helicities in proximity to each other. In the absence of Rashba spin-orbit coupling, the red (blue) arrows indicate movers with up (down) spin. The corresponding fermion fields are labeled on the top of this illustration. The interactions t_e, t_{2e}, and t_σ are "spin-preserving" processes; $t_{e'}$ and $t_{\sigma'}$ perturbations correspond to "spin-flip" processes which require Rahsba spin-orbit coupling.

The t_σ and $t_{\sigma'}$ processes can be viewed as "spin-flip" processes. In particular, $t_{\sigma'}$ operator breaks the non-generic spin S_z conservation[29]. These two interactions are analogous to the primary inter-edge interactions in the studies of helical liquid drag[52,53]. When t_σ and $t_{\sigma'}$ are both relevant, the junction becomes a barrier that suppresses electrical conduction and breaks time-reversal symmetry[29].

In the presence of time-reversal symmetry one can also consider an interaction-assisted backscattering[52]

$$\begin{aligned} H^{(\mathrm{irr})}_{\mathrm{junc}} = &- W'_+\Big[R^\dagger_-(0)L_-(0)R^\dagger_+(0)R_+(0) \\ &\quad - L^\dagger_-(0)R_-(0)L^\dagger_+(0)L_+(0) + \mathrm{H.c.}\Big] \\ &- W'_-\Big[R^\dagger_+(0)L_+(0)R^\dagger_-(0)R_-(0) \\ &\quad - L^\dagger_+(0)R_+(0)L^\dagger_-(0)L_+(0) - \mathrm{H.c.}\Big]. \end{aligned} \tag{13}$$

However, standard RG analysis shows that it and all other perturbations are irrelevant. Thus, in the remaining discussion we will focus on $H_{\mathrm{hLL},2} + H^{(1)}_{\mathrm{junc}} + H^{(2)}_{\mathrm{junc}} + H^{(I)}_{\mathrm{juct}}$, processes, summarized in Fig. 3.

In order to study above processes in the presence of Luttinger liquid interactions, we employ standard bosonization[47,48] of above Hamiltonian. With the detailed derivation relegated to Appendix B, below we summarize the results of the leading order renormalization group analysis, with the RG flow equations given by

$$\frac{dt_e}{dl} = \left[1 - \frac{1}{2}\left(K + \frac{1}{K}\right)\right] t_e, \tag{14a}$$

$$\frac{dt_{e'}}{dl} = \left[1 - \frac{1}{2}\left(K + \frac{1}{K}\right)\right] t_{e'}, \tag{14b}$$

$$\frac{dt_{2e}}{dl} = \left[1 - \frac{2}{K}\right] t_{2e}, \tag{14c}$$

$$\frac{dt_\sigma}{dl} = [1 - 2K]\, t_\sigma, \tag{14d}$$

$$\frac{dt_{\sigma'}}{dl} = [1 - 2K]\, t_{\sigma'}. \tag{14e}$$

These are consistent with the previous works on the corner junction[46] and the quantum point contact[29]. We also note that t_e and $t_{e'}$ are at most marginal in the noninteracting limit, $K = 1$. This ensures that the configuration of two helical states we consider is unchanged in the repulsive interaction regime. The Cooper pair tunneling t_{2e} naturally becomes relevant for sufficiently strong attractive interactions ($K > 2$). Thus, below we focus on the two-particle backscattering, t_σ and $t_{\sigma'}$, that become relevant for $K < 1/2$.

For such strongly repulsive interactions, $K < 1/2$, we only need to consider $H_{\mathrm{hLL},2} + H^{(I)}_{\mathrm{junc}}$. As detailed in Appendix B, the inter-domain-wall coupling decomposes the action into symmetric and antisymmetric sectors. In each sector, the action can be mapped to the Kane-Fisher model[54,55] with $K \to 2K$. For $K < 1/2$, the impurity interactions effectively cut (i.e., pin) the symmetric and antisymmetric Luttinger liquids. In the physical basis of two helical Luttinger liquids, the junction coupling creates a perfectly reflecting boundary condition which suppresses all conduction[29]. The junction is therefore "clogged." Concomitantly, the time-reversal symmetry is broken spontaneously and heterogeneously by the network of junctions[29].

At the critical point $K = 1/2$, the transmission across a single junction is nonzero and can be computed exactly by fermionizing the symmetric and antisymmetric sectors into a noninteracting model of Luther-Emery fermions. The scattering problem can then be solved exactly, with the physical transmission (T) and reflection (R) coefficients given by[29],

$$\mathrm{T} = \left(\frac{2e^{|M_b|/v}}{e^{2|M_b|/v} + 1}\right)^2, \tag{15a}$$

$$\mathrm{R} = \left(\frac{e^{2|M_b|/v} - 1}{e^{2|M_b|/v} + 1}\right)^2, \tag{15b}$$

where $b = S, A$ indicates symmetric and antisymmetric sectors. Above, $M_S = t_\sigma/(\pi\alpha)$ and $M_A = t_{\sigma'}/(\pi\alpha)$, with α the ultraviolet length-scale cutoff. We note that the expressions are independent of the energy due to low-energy point-scattering approximation. When $|M_b|/v \gg 1$, the transmission $\mathrm{T} \approx 4\exp(-2|M_b|/v)$. Therefore, we conclude that the junction at $K = 1/2$ is also clogged

for $|M_b|/v \gg 1$. The details of this analysis, extended beyond a point junction limit is relegated to Appendix B.

Above results can now be bootstrapped to characterize the helical network surface of clogged junctions. The surface can be viewed as a network of ideal helical conductors that are connected by clogged resistive junctions. Each clogged junction contributes incoherently a suppression factor $G_j \sim \exp(-2|M_j|/v)$, where j is the junction index and $|M_j|$ is the amplitude of the effective potential. The conductance is determined by the most conductive path in the network. We estimate the conductance by $G \sim \prod_j' G_j \sim \exp\left(-2\sum_j' |M_j|/v\right)$, where the summation runs over all the junctions in the most conductive path. Without loss of generality, the number of the junctions in the path is roughly $L/l_{\rm seg}$ ($l_{\rm seg}$ the typical length of the domain-wall segment). Combining above estimates, we predict a surface conductance $G \sim \exp(-2\frac{\bar{M}}{v}\frac{L}{l_{\rm seg}})$ where $\bar{M}$ is the averaged value of $|M_j|$. As a comparison, the conductance in the localized regime is $G \sim \exp(-2L/\xi_{\rm loc})$, where $\xi_{\rm loc}$ is the averaged localization length. The exponentially small conductance of the clogged state and the absence of qualitative distinctions, argues that these regimes are a single localized state, separated by a smooth crossover, rather than a genuine phase transition.

V. DISCUSSION AND SUMMARY

We explored the stability of a 2D metallic surface of a 3D spin chiral (CII class) topological insulator to disorder and interaction. In the scenario of a symmetry broken surface that forms multiple statistically symmetric domains, we argued that the surface can realize a *gapless insulating* ground state, with two regimes - a network of 1D helical domain-walls interrupted by blockaded junctions (the clogged regime), and a network of localized 1D helical channels (the fully-localized regime). This gapless insulating surface state, realized only in the CII TI class, is a distinct scenario from the previously discussed possibilities of interacting TI surfaces[9–13].

The gapless insulating surface of nontrivial TIs predicted here shares many experimental features with a 2D conventional Anderson insulator, exhibiting vanishing dc conductivity and nonzero compressibility. However, it may be distinguishable through real-space surface imaging (e.g., STM) by its low-energy states organized into the characteristic domain-wall network, quite different from the conventional 2D localized states. In addition, the half-charge excitations in the localized regime[16] and the perfect barrier junctions[29] should in principle be experimentally detectable via noise measurements.

Finite temperature and finite frequency measurements may also be able to distinguish between the clogged and fully-localized regimes, tunable by the strength of interactions and disorder, with the latter controlling the domain size. In the clogged regime of the dilute domain-wall limit the temperature dependence of the surface transport is dictated by the weak junction links[54,55] and should then exhibit the one-dimensional insulator dependence. The ac conductivity will show a crossover frequency scale set by $\omega^* \sim v_F/l_{\rm seg}$ ($l_{\rm seg}$ the length of domain-wall segment) above which the ac conductivity is the same as that of a 1D helical liquid[56]. In contrast, at low frequency ($\omega < \omega^*$) the ac conductivity should vanish due to the weak link barriers at the junctions.

In the fully-localized regime, the transport is governed by a network of one-dimensional localized insulators. The low temperature conductance due to a localized insulator should follow $G \sim e^{-2L/\xi_{\rm loc}}$, where $\xi_{\rm loc}$ is the localization length. The ac conductivity should show the Mott conductivity $\sigma \propto \omega^2$[57] up to logarithmic corrections. These two regimes are connected via a crossover for finite domain-wall segments and become distinct phases in the infinite domain-wall segment limit.

In this work, we consider statistically symmetry-preserving disorder that creates inhomogeneous symmetry breaking. Such disorder may be generated due to the interplay of symmetric disorder and interaction, leading to instabilities of the dirty interacting topological surface states[58–60]. A systematic derivation of the heterogeneous spontaneous symmetry breaking in a dirty interacting TI is beyond the scope of the current work and is left to future studies.

We note that the clogged state predicted here may also be realized in the Luttinger liquid networks of the (twisted) bilayer graphene and other related platforms[61–72]. If so, the clogged phenomenology predicted here may extend to those systems as well. We leave to future work the extension of the present analysis to six-way junctions, relevant in the twisted bilayer graphene systems[63,64].

ACKNOWLEDGMENT

We thank Matthew Foster, Jason Iaconis, Han Ma, Itamar Kimchi, and Abhinav Prem for useful discussions. This work is supported in part by a Simons Investigator award from the Simons Foundation (Y.-Z.C. and L.R.), and in part by the Army Research Office under Grant Number W911NF-17-1-0482 (Y.-Z.C. and R.M.N.). Part of this work was performed (Y.-Z.C. and R.M.N.) at the KITP, supported by the NSF under Grant No. PHY-1748958. The views and conclusions contained in this document are those of the authors and should not be interpreted as representing the official policies, either expressed or implied, of the Army Research Office or the U.S. Government. The U.S. Government is authorized to reproduce and distribute reprints for Government purposes notwithstanding any copyright notation herein.

Appendix A: Derivations of domain-wall states

Here we derive the low-energy domain-wall model from the 2D surface theory encoded in $H_0 + H_{\rm dis} + H_{{\rm M},a}$, Eqs. (1), (2), and (4). Our strategy is to first solve $H_0 + H_{{\rm M},a}$ exactly, thereby obtaining the domain-wall states and then treat $H_{\rm dis}$ as a perturbation. The solution of $H_0 + H_{{\rm M},a}$ can be parametrized by $\Psi_0(x,y) = f(x)\left[\tilde{\psi}_1(y)\hat{v}_1 + \tilde{\psi}_2(y)\hat{v}_2\right]$ where $\tilde{\psi}_{1,2}(y)$ are normalized wavefunctions of y and $\hat{v}_{1,2}$ is a four component vector. Taking $m_a(x) = m_a\,{\rm sgn}(x)$, we find that the amplitude $f(x)$ and vectors $\hat{v}_{1,2}$ satisfy,

$$-iv_D\hat{\sigma}^x\hat{v}_{1,2}\partial_x f(x) + m_a\,{\rm sgn}(x)\hat{M}_a\hat{v}_{1,2}f(x) = 0, \quad \text{(A1)}$$

that reduces to

$$\hat{v}_{1,2}\partial_x f(x) = -\frac{m_a}{v_D}\left(i\hat{\sigma^x}\hat{M}_a\right){\rm sgn}(x)\hat{v}_{1,2}f(x). \quad \text{(A2)}$$

The zero energy normalizable amplitude solution is given by

$$f(x) = \sqrt{\frac{m_a}{v_D}}e^{-(m_a/v_D)|x|}, \quad \text{(A3)}$$

and the four component vectors satisfy

$$i\hat{\sigma}^x\hat{M}_a\hat{v}_{1,2} = \hat{v}_{1,2}. \quad \text{(A4)}$$

The above solution $f(x)$ describes the domain-wall profile across x, with the domain-wall chosen to run along y. The single domain-wall assumption is justified as long as its width (v_D/m_a) is much smaller than the typical domain size w, i.e., $wm_a/v_D \gg 1$.

To obtain the effective 1D domain-wall Hamiltonian we substitute Ψ_0 for Ψ inside $H_0 + H_{\rm dis} + H_{{\rm M},a}$. The resulting kinetic energy part of the domain-wall Hamiltonian is then given by

$$\begin{aligned} H_{\rm DW,0} &= \left[H_0 + H_{{\rm M},a}\right]_{\Psi\to\Psi_0} \\ &= v_D\int dy\left[-is_1\tilde{\psi}_1^\dagger\partial_y\tilde{\psi}_1 - is_2\tilde{\psi}_2^\dagger\partial_y\tilde{\psi}_2\right], \end{aligned} \quad \text{(A5)}$$

where $s_{1,2} = \hat{v}_{1,2}^\dagger\hat{\sigma}^y\hat{v}_{1,2} = \pm 1$ determines the sign of velocities for the fermion fields ψ_i. The domain-wall model is chiral when $s_1 = s_2$. We note that there is no mixing term because $[\hat{\sigma}^x\hat{M}_a, \hat{\sigma}^y] = 0$.

The disorder part of the Hamiltonian is given by

$$\begin{aligned} &H_{\rm DW,dis} = H_{\rm dis}\left[\Psi\to\Psi_0\right], \\ &= \sum_{a,b}\int dy\,\tilde{\psi}_a^\dagger\hat{v}_a^\dagger\left[\tilde{v}_1\hat{\tau}^x + \tilde{v}_2\hat{\tau}^z + \tilde{a}_1\hat{\sigma}^x\hat{\tau}^y + \tilde{a}_2\hat{\sigma}^y\hat{\tau}^y\right]\hat{v}_b\tilde{\psi}_b, \end{aligned} \quad \text{(A6)}$$

where $a, b = 1, 2$ are the one-dimensional fermion flavors. The 1D disorder bilinears, $\tilde{v}_1$, $\tilde{v}_2$, $\tilde{a}_1$, and $\tilde{a}_2$, correspond to their 2D disorder counter-parts, v_1, v_2, a_1, and a_2, respectively, related by, $\tilde{\mathcal{O}}(y) = \int dx f^2(x)\mathcal{O}(x,y)$ for $\mathcal{O} = v_1, v_2, a_1, a_2$.

We now use this set up to derive and analyze the structure of the chiral, helical, and (fine-tuned) non-topological domain-walls.

1. Chiral domain-walls

In the presence of only $\hat{M}_1 = \hat{\sigma}^z$ mass operator, the time-reversal symmetry ($\mathcal{T}$) is broken, but the particle-hole ($\mathcal{P}$) is preserved. The resulting symmetry-broken surface corresponds to the symmetry class C[73]. The corresponding spinor equation reduces to $i\hat{\sigma}^x\hat{M}_1\hat{v}_{1,2} = \hat{\sigma}^y\hat{v}_{1,2} = \hat{v}_{1,2}$, with solutions

$$\hat{v}_1 = \frac{1}{\sqrt{2}}\begin{bmatrix}1\\0\\i\\0\end{bmatrix}, \ \hat{v}_2 = \frac{1}{\sqrt{2}}\begin{bmatrix}0\\1\\0\\i\end{bmatrix}. \quad \text{(A7)}$$

We can then identify that $s_1 = \hat{v}_1^\dagger\hat{\sigma}^y\hat{v}_1 = 1$ and $s_2 = \hat{v}_2^\dagger\hat{\sigma}^y\hat{v}_2 = 1$. Based on the structure in Eq. (A5), the domain-wall state only contains right-mover fermions. Thus such a domain-wall solution realizes a chiral state, which corresponds to the spin quantum Hall edge of class C[37–40], and is robust against any local perturbation within a domain-wall.

For completeness, we also construct the disorder potential on the domain-wall even though a chiral state is robust against such disorder. Using Eqs. (A6) and (A7), the effective disorder domain-wall Hamiltonian is given by

$$H^{(1)}_{\rm DW,dis} = \int_y\left[\tilde{v}_2(y)(\psi_1^\dagger\psi_1 - \psi_2^\dagger\psi_2) + \tilde{a}_2(y)(i\psi_2^\dagger\psi_1 - i\psi_1^\dagger\psi_2)\right].$$

Above $\tilde{v}_2$ plays the role of an anti-symmetric chemical potential in the two right movers, and $\tilde{a}_y$ is an impurity forward scattering between two right movers, that cannot induce localization[74].

2. Helical domain-walls

We now consider a symmetry-breaking mass $\hat{M}_2 = \hat{\sigma}^z\hat{\tau}^y$. This mass bilinear breaks the particle-hole symmetry but preserves time-reversal symmetry. The symmetry-broken surface belongs to the class AII (the same as the 2D time-reversal symmetric Z_2 TIs). The corresponding spinor equation is $\hat{\sigma}^y\hat{\tau}^y\hat{v}_{1,2} = \hat{v}_{1,2}$ yields solutions

$$\hat{v}_1 = \frac{1}{2}\begin{bmatrix}1\\i\\i\\-1\end{bmatrix}, \ \hat{v}_2 = \frac{1}{2}\begin{bmatrix}1\\-i\\-i\\-1\end{bmatrix}. \quad \text{(A8)}$$

In this case, $s_1 = \hat{v}_1^\dagger\hat{\sigma}^y\hat{v}_1 = 1$ and $s_2 = \hat{v}_2^\dagger\hat{\sigma}^y\hat{v}_2 = -1$. According to Eq. (A5), the domain-wall movers are described by a right mover ($s_1 = 1$) and a left mover ($s_2 = -1$). In order to assess the effect of symmetric

disorder, we construct the domain-wall disorder potential Hamiltonian based on Eq. (A6), obtaining

$$H^{(2)}_{\rm DW,dis} = \int_y \tilde{a}_2(y) \left[\tilde{\psi}_1^\dagger \tilde{\psi}_1 + \tilde{\psi}_2^\dagger \tilde{\psi}_2\right]. \tag{A9}$$

The domain-wall disorder is controlled by a scalar potential $\tilde{a}_2$, corresponding to a randomly fluctuating chemical potential. Based on symmetry, one can also include $\hat{V}_4 = \hat{1}$ in Table I. This only creates correction to the existing random chemical potential fluctuation. There are no additional bilinear operators with $\mathcal{T}^2 = -1$, so we conclude that the domain-wall state is a helical state[28] which is topological protected from disorder in the absence of interactions[17].

3. Normal domain-wall

For certain microscopic models (e.g., fine tuning interactions such that only $U_3 \neq 0$ or $U_4 \neq 0$ appear), it is possible to realize only one mass term. Here, we perform the same analysis to derive the domain-wall states due to only $\hat{M}_3 = \hat{\sigma}^z\hat{\tau}^x$ or $\hat{M}_4 = \hat{\sigma}^z\hat{\tau}^z$ mass operators. In the two dimensions, the AIII class is topologically trivial. The spinor solutions ($\hat{v}_{1,2}$ for $\hat{M}_3$, $\hat{u}_{1,2}$ for $\hat{M}_4$) obey $\hat{\sigma}^y\hat{\tau}^x\hat{v}_{1,2} = \hat{v}_{1,2}$ and $\hat{\sigma}^y\hat{\tau}^z\hat{u}_{1,2} = \hat{u}_{1,2}$. The corresponding solutions are given by

$$\hat{v}_1 = \frac{1}{2}\begin{bmatrix} 1 \\ 1 \\ i \\ i \end{bmatrix}, \quad \hat{v}_2 = \frac{1}{2}\begin{bmatrix} 1 \\ -1 \\ -i \\ i \end{bmatrix}, \tag{A10}$$

and

$$\hat{u}_1 = \frac{1}{\sqrt{2}}\begin{bmatrix} 1 \\ 0 \\ i \\ 0 \end{bmatrix}, \quad \hat{u}_2 = \frac{1}{\sqrt{2}}\begin{bmatrix} 0 \\ 1 \\ 0 \\ -i \end{bmatrix} \tag{A11}$$

We thus identify that $\hat{v}_1^\dagger\hat{\sigma}^y\hat{v}_1 = \hat{u}_1^\dagger\hat{\sigma}^y\hat{u}_1 = 1$ (right mover) and $\hat{v}_2^\dagger\hat{\sigma}^y\hat{v}_2 = \hat{u}_2^\dagger\hat{\sigma}^y\hat{u}_2 = -1$ (left mover). Therefore, both cases give a non-chiral state. Because the surface state is in class A, the massless domain-wall hosts non-topological 1D fermions.

For completeness, we also discuss the corresponding domain-wall disorder. With the mass $\hat{M}_3$, the disorder part is given by

$$H^{(3)}_{\rm DW,dis} = \int_y \tilde{v}_1(y) \left[\tilde{\psi}_1^\dagger \tilde{\psi}_1 - \tilde{\psi}_2^\dagger \tilde{\psi}_2\right] + \int_y \tilde{a}_1(y) \left[\tilde{\psi}_2^\dagger \tilde{\psi}_1 + \tilde{\psi}_1^\dagger \tilde{\psi}_2\right]. \tag{A12}$$

For $\hat{M}_4$ case we instead find,

$$H^{(4)}_{\rm DW,dis} = \int_y \tilde{v}_2(y) \left[\tilde{\psi}_1^\dagger \tilde{\psi}_1 - \tilde{\psi}_2^\dagger \tilde{\psi}_2\right] - \int_y \tilde{a}_1(y) \left[\tilde{\psi}_2^\dagger \tilde{\psi}_1 + \tilde{\psi}_1^\dagger \tilde{\psi}_2\right]. \tag{A13}$$

The antisymmetry chemical potentials ($\tilde{v}_1$ in $H^{(3)}_{\rm DW,dis}$ and $\tilde{v}_2$ in $H^{(4)}_{\rm DW,dis}$) couples to the difference of right and left mover local densities. Both cases allow for conventional impurity backscattering ($\tilde{a}_1$ in both cases) within the domain wall, and thus realizes topologically trivial 1D fermions, which are therefore not protected against Anderson localization.

Appendix B: Helical junction

In this appendix, we provide the derivations of the results in Sec. IV B. We will also review the standard bosonization and the Luther-Emery analysis.

1. Bosonization

In order to treat the Luttinger interaction nonperturbatively, we adopt the standard field theoretic bosonization method[48]. The fermionic fields can be described by chiral bosons via

$$R_a(x) = \frac{\hat{U}_a}{\sqrt{2\pi\alpha}} e^{i[\phi_a+\theta_a](x)}, \; L_a(x) = \frac{\hat{U}_a}{\sqrt{2\pi\alpha}} e^{i[\phi_a-\theta_a](x)}, \tag{B1}$$

where $\phi_{a=\pm}$ is the bosonic phase field, $\theta_{a=\pm}$ is the phonon-like boson, $U_{a=\pm}$ is the Klein factor[47], and α is the ultraviolet length scale that is determined by the microscopic model. The time-reversal operation ($\mathcal{T}^2 = -1$) in the bosonic language is defined as follows: $\phi_\pm \to -\phi_\pm + \frac{\pi}{2}$, $\theta_\pm \to \theta_\pm - \frac{\pi}{2}$, and $i \to -i$. This corresponds to the fermionic operation $R_\pm \to L_\pm$, $L_\pm \to -R_\pm$, and $i \to -i$. We note that the introduction of the Klein factors ($U_{a=\pm}$) here is just for bookkeeping purpose.

Now, we perform the standard bosonization and analyze the Hamiltonian. The Hamiltonian of each helical liquid is bosonized to

$$H_{\rm hLL,2} = \sum_{a=\pm}\int_x \left[\frac{v}{2\pi K}\left(\partial_x\theta_a\right)^2 + \frac{vK}{2\pi}\left(\partial_x\phi_a\right)^2\right], \tag{B2}$$

where we have assumed the same velocity (v) and the same Luttinger parameter (K) among the two helical liquids. K encodes the strength Luttinger liquid interactions. $K < 1$ ($K > 1$) for repulsive (attractive) interactions. $K = 1$ is at the non-interacting fermion limit.

The impurity perturbations [given by Eqs. (10), (11), and (12)] are bosonized to

$$H^{(1)}_{\rm junc} = -\frac{t_e}{2\pi\alpha}\left[\hat{U}^\dagger_-\hat{U}_+(2i)e^{i(\phi_+-\phi_-)}\sin(\theta_++\theta_-)+\text{H.c.}\right] - \frac{t_{e'}}{2\pi\alpha}\left[\hat{U}^\dagger_-\hat{U}_+2e^{i(\phi_+-\phi_-)}\cos(\theta_+-\theta_-)+\text{H.c.}\right], \tag{B3}$$

$$H^{(2)}_{\rm junc} = -\frac{t_{2e}}{4\pi\alpha^2}\left[\hat{U}^\dagger_-\hat{U}^\dagger_-\hat{U}_+\hat{U}_+e^{i(2\phi_+-2\phi_-)}+\text{H.c.}\right], \tag{B4}$$

$$H^{(I)}_{\rm junc} = -\frac{t_\sigma}{2\pi^2\alpha^2}\cos[2\theta_++2\theta_-]-\frac{t_{\sigma'}}{2\pi^2\alpha^2}\cos[2\theta_+-2\theta_-]. \tag{B5}$$

The corresponding renormalization group equations can be found in Eq. (14).

2. Clogged junction

We are interested in the repulsive interacting regime ($K<1$) in the helical network model. Therefore, we focus on the t_σ and $t_{\sigma'}$ interactions given by Eq. (B5) and ignore other processes. In the strong coupling limit ($K<1/2$), the ground state constraints are $\theta_+(t,x=0)+\theta_-(t,x=0)=n\pi$ and $\theta_+(t,x=0)+\theta_-(t,x=0)=m\pi$ where n and m are integers. The ground state yields static solutions at $x=0$: $\theta_+(t,x=0)=(n+m)\pi/2$ and $\theta_-(t,x=0)=(n-m)\pi/2$. As a consequence, the current $I_\pm=-\frac{1}{\pi}\partial_t\theta_\pm$ at $x=0$ is zero in both of the helical liquids. Therefore, we predict that a four-way junction with semi-infinite helical liquids becomes "clogged" for $K<1/2$.

An alternative way to view the clogging is to map the problem to a modified Kane-Fisher single impurity problem[54,55]. We define symmetric and anti-symmetric collective bosonic modes as follows:

$$\Theta_S=\frac{1}{\sqrt{2}}(\theta_++\theta_-),\ \Phi_S=\frac{1}{\sqrt{2}}(\phi_++\phi_-), \tag{B6}$$

$$\Theta_A=\frac{1}{\sqrt{2}}(\theta_+-\theta_-),\ \Phi_A=\frac{1}{\sqrt{2}}(\phi_+-\phi_-). \tag{B7}$$

The subscript S and A denote the symmetric and anti-symmetric collective modes respectively. Now, we use the collective coordinate to rewrite the theory. The Luttinger liquid Hamiltonian in Eq. (B2) is now expressed by

$$H_{\rm hLL,2}=\int_x\left[\frac{v}{2\pi K}(\partial_x\Theta_S)^2+\frac{vK}{2\pi}(\partial_x\Phi_S)^2\right] \tag{B8}$$

$$+\int_x\left[\frac{v}{2\pi K}(\partial_x\Theta_A)^2+\frac{vK}{2\pi}(\partial_x\Phi_A)^2\right]. \tag{B9}$$

We note that the impurity interaction can not induce renormalization of the velocity and Luttinger parameter. The junction interactions in Eq. (B5) becomes to

$$H^{(I)}_{\rm junc}=-\frac{t_\sigma}{2\pi^2\alpha^2}\cos\left[2\sqrt{2}\Theta_S\right]-\frac{t_{\sigma'}}{2\pi^2\alpha^2}\cos\left[2\sqrt{2}\Theta_A\right]. \tag{B10}$$

Both the symmetric and anti-symmetric sectors can be individually mapped to the Kane-Fisher problem[54,55] with $K\to 2K$. The critical point is given by $K=1/2$ below which the transmission of both the symmetric and anti-symmetric modes vanish to zero.

3. Luther-Emery Analysis

At the critical point $K=1/2$, one can perform standard refermionization for the two helical Luttinger liquids problem since both the symmetric and the anti-symmetric sectors correspond to the Kane-Fisher model[54,55]. We introduce the Luther-Emery fermions via

$$\Psi_{b,R}(x)=\frac{e^{i\left[\Phi_b(x)/\sqrt{2}+\sqrt{2}\Theta_b(x)\right]}}{\sqrt{2\pi\alpha}},$$
$$\Psi_{b,L}(x)=\frac{e^{i\left[\Phi_b(x)/\sqrt{2}-\sqrt{2}\Theta_b(x)\right]}}{\sqrt{2\pi\alpha}}, \tag{B11}$$

where $b=S,A$ is the index for symmetric (S) and antisymmetric (A) collective modes. The Luther-Emery fermion Hamiltonian of the sector b is given by

$$H_b=-iv\int dx\left[\Psi^\dagger_{b,R}\partial_x\Psi_{b,R}-\Psi^\dagger_{b,L}\partial_x\Psi_{b,L}\right] + M_b\left[\Psi^\dagger_{b,R}\Psi_{b,L}+\Psi^\dagger_{b,L}\Psi_{b,R}\right]_{x=0}, \tag{B12}$$

where $M_{b=S}=t_\sigma/(\pi\alpha)$ and $M_{b=A}=t_{\sigma'}/(\pi\alpha)$. The impurity mass problem can be solved via standard quantum mechanical scattering approach. Firstly, we derive the Dirac equation as follows:

$$\begin{bmatrix}-iv\partial_x & M_b\delta(x)\\ M_b\delta(x) & iv\partial_x\end{bmatrix}\begin{bmatrix}\Psi_{b,R}\\ \Psi_{b,L}\end{bmatrix}=E\begin{bmatrix}\Psi_{b,R}\\ \Psi_{b,L}\end{bmatrix} \tag{B13}$$

$$\to -iv\hat{\sigma}^z\partial_x\hat{\Psi}_b+M_b\delta(x)\hat{\sigma}^x\hat{\Psi}_b=E\hat{\Psi}_b, \tag{B14}$$

where $\hat{\Psi}_b$ is the two-component column vector that contains $\Psi_{b,R}$ and $\Psi_{b,L}$. The above equation satisfies a boundary condition as follows:

$$-iv\hat{\sigma}^z\left[\hat{\Psi}_b(0^+)-\hat{\Psi}_b(0^-)\right]+M_b\hat{\sigma}^x\hat{\Psi}_b(0)=0. \tag{B15}$$

We note that this boundary condition is ambiguous because the wavefunction might be discontinuous at $x=0$.

Instead of studying the delta distribution problem, we replace the impurity potential by a square well potential, $M_b\delta(x)\to\tilde{M}_b\Theta(x)\Theta(d-x)$, where d is the size of mass

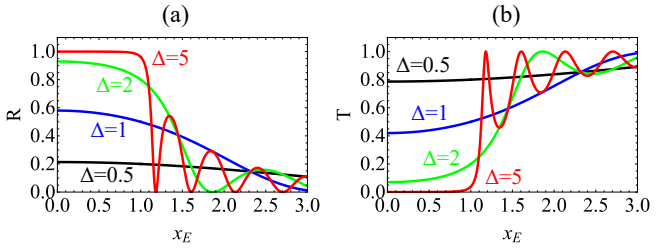

FIG. 4. Reflection and transmission of 1D Dirac scattering problem (finite mass region) as functions of rescaled energy. (a) Reflection, $\mathrm{R} = |A|^2$. (b) Transmission, $\mathrm{T} = |D|^2$. Both A and B are given by Eq. (B21). x_E is the dimensionless energy parameter defined in the text below Eq. (B21). Black, blue, green, and red curves indicate $\Delta = M_b/v = 0.5, 1, 2, 5$ respectively. The perfect transmissions (T= 1 and R= 0) for $x_E > 1$ correspond to the Fabry-Pérot interference.

region and $\tilde{M}_b = M_b/d$ is the "mass" strength. The impurity limit is obtained by taking $d \to 0^+$. With a finite d, the wavefunction is continuous everywhere because of the analyticity. We consider a scattering ansatz as follows:

$$\hat{\Psi}_b(x) = \begin{cases} e^{ikx}\begin{bmatrix}1\\0\end{bmatrix} + Ae^{-ikx}\begin{bmatrix}0\\1\end{bmatrix}, & \text{for } x \le 0, \\ Be^{iqx}\begin{bmatrix}1\\\frac{-vq+E}{\tilde{M}_b}\end{bmatrix} + Ce^{-iqx}\begin{bmatrix}\frac{-vq+E}{\tilde{M}_b}\\1\end{bmatrix}, & \text{for } 0 < x \le d, \\ De^{ikx}\begin{bmatrix}1\\0\end{bmatrix}, & \text{for } x > d, \end{cases} \tag{B16}$$

where $k = E/v$ and $q = \sqrt{E^2 - \tilde{M}_b^2}/v$. The boundary conditions are given by

$$B + C\left(\frac{-vq+E}{\tilde{M}_b}\right) = 1, \tag{B17}$$

$$B\left(\frac{-vq+E}{\tilde{M}_b}\right) + C = A, \tag{B18}$$

$$Be^{iqd} + Ce^{-iqd}\left(\frac{-vq+E}{\tilde{M}_b}\right) = De^{ikd}, \tag{B19}$$

$$Be^{iqd}\left(\frac{-vq+E}{\tilde{M}_b}\right) + Ce^{-iqd} = 0. \tag{B20}$$

With the help of Mathematica, one can obtain the solutions as follows:

$$A = \frac{\left(\sqrt{x_E^2-1} - x_E\right)\left(-1 + e^{2i\Delta\sqrt{x_E^2-1}}\right)}{1 + \left(2x_E\sqrt{x_E^2-1} - 2x_E^2 + 1\right)e^{2i\Delta\sqrt{x_E^2-1}}}, \tag{B21a}$$

$$B = \frac{1}{1 + \left(2x_E\sqrt{x_E^2-1} - 2x_E^2 + 1\right)e^{2i\Delta\sqrt{x_E^2-1}}}, \tag{B21b}$$

$$C = \frac{\left(\sqrt{x_E^2-1} - x_E\right)e^{2i\Delta\sqrt{x_E^2-1}}}{1 + \left(2x_E\sqrt{x_E^2-1} - 2x_E^2 + 1\right)e^{2i\Delta\sqrt{x_E^2-1}}}, \tag{B21c}$$

$$D = \frac{2\left(x_E\sqrt{x_E^2-1} - x_E^2 + 1\right)e^{i\Delta\left(\sqrt{x_E^2-1} - x_E\right)}}{1 + \left(2x_E\sqrt{x_E^2-1} - 2x_E^2 + 1\right)e^{2i\Delta\sqrt{x_E^2-1}}}, \tag{B21d}$$

where $x_E \equiv E/|\tilde{M}_b|$ and $\Delta \equiv d|\tilde{M}_b|/v = |M_b|/v$. The reflection is $\mathrm{R} = |A|^2$ and transmission is $\mathrm{T} = |D|^2$. The dependence of x_E and Δ are plotted in Fig. 4. For $\Delta = |M_b|/v \gg 1$, the scattering problem reveals a sharp gap structure because $\mathrm{R} \approx 1$ for $x_E < 1$. For $x_E > 1$, there are some special energies that allow perfect transmission. This is related to the Fabry-Pérot interference. However, we do not focus on such high energy phenomenon in this work.

Now, we consider $d \to 0^+$ with $\tilde{M}_b d = M_b$ fixed. The finite mass region is reduced to a single impurity potential. In the impurity case, $x_E = Ed/|M_b| \to 0$ for a fixed M_b/v. The expression of transmission and reflection are reduced to Eq. (15). The results do not depend on the energy due to the infinite $|\tilde{M}_b| = |M_b|/d$ in this limit. These results characterize the low energy scattering in the network model. In particular, the transmission $\mathrm{T} \to 4e^{-2|M_b|/v}$ when $|M_b|/v \gg 1$.

In the four-way junction problem, the clogging conditions at $K = 1/2$ correspond to perfect reflections in both the symmetric and antisymmetric sectors. In the zero energy limit, the clogging conditions are $|M_S|/v \gg 1$ and $|M_A|/v \gg 1$. To make the junction more realistic, we can assume that both the domain-wall segment and the interacting region are finite. The longest wavelength is set by the typical domain-wall segment length, l_{seg}, corresponding to the lowest kinetic energy $E_0 = v(2\pi/l_{\mathrm{seg}})$. The clogging conditions become to $v(2\pi/l_{\mathrm{seg}}) < |t_\sigma|/(\pi\alpha d)$, $v(2\pi/l_{\mathrm{seg}}) < |t_{\sigma'}|/(\pi\alpha d)$, $|t_\sigma|/(v\pi\alpha) \gg 1$, and $|t_{\sigma'}|/(v\pi\alpha) \gg 1$. The former two conditions are from comparing the energy of the electron to the local mass; the latter two conditions are related to the existence of sharp gaps.

* YangZhi.Chou@colorado.edu

[1] M. Z. Hasan and C. L. Kane, Rev. Mod. Phys. **82**, 3045

(2010).
[2] X.-L. Qi and S.-C. Zhang, Rev. Mod. Phys. **83**, 1057 (2011).
[3] C.-K. Chiu, J. C. Y. Teo, A. P. Schnyder, and S. Ryu, Rev. Mod. Phys. **88**, 035005 (2016).
[4] A. W. Ludwig, Physica Scripta **2016**, 014001 (2015).
[5] P. W. Anderson, Phys. Rev. **109**, 1492 (1958).
[6] F. Evers and A. D. Mirlin, Rev. Mod. Phys. **80**, 1355 (2008).
[7] Y. Ando and L. Fu, Annu. Rev. Condens. Matter Phys. **6**, 361 (2015).
[8] T. Mizushima, Y. Tsutsumi, T. Kawakami, M. Sato, M. Ichioka, and K. Machida, Journal of the Physical Society of Japan **85**, 022001 (2016), https://doi.org/10.7566/JPSJ.85.022001.
[9] A. Vishwanath and T. Senthil, Phys. Rev. X **3**, 011016 (2013).
[10] C. Wang and T. Senthil, Phys. Rev. B **87**, 235122 (2013).
[11] C. Wang and T. Senthil, Phys. Rev. B **89**, 195124 (2014).
[12] M. A. Metlitski, L. Fidkowski, X. Chen, and A. Vishwanath, arXiv preprint arXiv:1406.3032 (2014).
[13] T. Senthil, Annual Review of Condensed Matter Physics **6**, 299 (2015), https://doi.org/10.1146/annurev-conmatphys-031214-014740.
[14] C. Xu and J. E. Moore, Phys. Rev. B **73**, 045322 (2006).
[15] C. Wu, B. A. Bernevig, and S.-C. Zhang, Phys. Rev. Lett. **96**, 106401 (2006).
[16] Y.-Z. Chou, R. M. Nandkishore, and L. Radzihovsky, Phys. Rev. B **98**, 054205 (2018).
[17] C. L. Kane and E. J. Mele, Phy. Rev. Lett. **95**, 146802 (2005).
[18] C. L. Kane and E. J. Mele, Phy. Rev. Lett. **95**, 226801 (2005).
[19] B. A. Bernevig and S.-C. Zhang, Phys. Rev. Lett. **96**, 106802 (2006).
[20] A. Luther and V. J. Emery, Phys. Rev. Lett. **33**, 589 (1974).
[21] L. Du, I. Knez, G. Sullivan, and R.-R. Du, Phys. Rev. Lett. **114**, 096802 (2015).
[22] T. Li, P. Wang, H. Fu, L. Du, K. A. Schreiber, X. Mu, X. Liu, G. Sullivan, G. A. Csáthy, X. Lin, and R.-R. Du, Phys. Rev. Lett. **115**, 136804 (2015).
[23] L. Du, T. Li, W. Lou, X. Wu, X. Liu, Z. Han, C. Zhang, G. Sullivan, A. Ikhlassi, K. Chang, and R.-R. Du, Phys. Rev. Lett. **119**, 056803 (2017).
[24] T. Li, P. Wang, G. Sullivan, X. Lin, and R.-R. Du, Phys. Rev. B **96**, 241406 (2017).
[25] T. Morimoto, A. Furusaki, and C. Mudry, Phys. Rev. B **91**, 235111 (2015).
[26] T. Morimoto, A. Furusaki, and C. Mudry, Phys. Rev. B **92**, 125104 (2015).
[27] X.-Y. Song and A. P. Schnyder, Phys. Rev. B **95**, 195108 (2017).
[28] A. C. Potter, C. Wang, M. A. Metlitski, and A. Vishwanath, Phys. Rev. B **96**, 235114 (2017).
[29] J. C. Y. Teo and C. L. Kane, Phys. Rev. B **79**, 235321 (2009).
[30] A. P. Schnyder, S. Ryu, A. Furusaki, and A. W. W. Ludwig, Phys. Rev. B **78**, 195125 (2008).
[31] P. Hosur, S. Ryu, and A. Vishwanath, Phys. Rev. B **81**, 045120 (2010).
[32] S. Ryu, C. Mudry, A. W. W. Ludwig, and A. Furusaki, Phys. Rev. B **85**, 235115 (2012).
[33] A. W. W. Ludwig, M. P. A. Fisher, R. Shankar, and G. Grinstein, Phys. Rev. B **50**, 7526 (1994).
[34] I. C. Fulga, B. van Heck, J. M. Edge, and A. R. Akhmerov, Phys. Rev. B **89**, 155424 (2014).
[35] R. Jackiw and C. Rebbi, Phys. Rev. D **13**, 3398 (1976).
[36] W. P. Su, J. R. Schrieffer, and A. J. Heeger, Phys. Rev. Lett. **42**, 1698 (1979).
[37] I. A. Gruzberg, N. Read, and S. Sachdev, Phys. Rev. B **55**, 10593 (1997).
[38] T. Senthil, M. P. A. Fisher, L. Balents, and C. Nayak, Phys. Rev. Lett. **81**, 4704 (1998).
[39] I. A. Gruzberg, A. W. W. Ludwig, and N. Read, Phys. Rev. Lett. **82**, 4524 (1999).
[40] T. Senthil, J. B. Marston, and M. P. A. Fisher, Phys. Rev. B **60**, 4245 (1999).
[41] H.-Y. Xie, H. Li, Y.-Z. Chou, and M. S. Foster, Phys. Rev. Lett. **116**, 086603 (2016).
[42] H. Obuse, A. Furusaki, S. Ryu, and C. Mudry, Phys. Rev. B **76**, 075301 (2007).
[43] H. Obuse, A. Furusaki, S. Ryu, and C. Mudry, Phys. Rev. B **78**, 115301 (2008).
[44] S. Ryu, C. Mudry, H. Obuse, and A. Furusaki, New Journal of Physics **12**, 065005 (2010).
[45] H. Obuse, S. Ryu, A. Furusaki, and C. Mudry, Phys. Rev. B **89**, 155315 (2014).
[46] C.-Y. Hou, E.-A. Kim, and C. Chamon, Phys. Rev. Lett. **102**, 076602 (2009).
[47] T. Giamarchi, *Quantum physics in one dimension* (Oxford Science Publications, 2004).
[48] R. Shankar, *Quantum Field Theory and Condensed Matter: An Introduction* (Cambridge University Press, 2017).
[49] V. L. Pokrovsky and A. L. Talapov, Phys. Rev. Lett. **42**, 65 (1979).
[50] M. Bocquet, Nuclear Physics B **546**, 621 (1999).
[51] Y. Tanaka and N. Nagaosa, Phys. Rev. Lett. **103**, 166403 (2009).
[52] Y.-Z. Chou, A. Levchenko, and M. S. Foster, Phys. Rev. Lett. **115**, 186404 (2015).
[53] Y.-Z. Chou, Phys. Rev. B **99**, 045125 (2019).
[54] C. L. Kane and M. P. A. Fisher, Phys. Rev. B **46**, 15233 (1992).
[55] C. L. Kane and M. P. A. Fisher, Phys. Rev. Lett. **68**, 1220 (1992).
[56] N. Kainaris, I. V. Gornyi, S. T. Carr, and A. D. Mirlin, Phys. Rev. B **90**, 075118 (2014).
[57] N. F. Mott, The Philosophical Magazine: A Journal of Theoretical Experimental and Applied Physics **17**, 1259 (1968), https://doi.org/10.1080/14786436808223200.
[58] M. S. Foster and E. A. Yuzbashyan, Phys. Rev. Lett. **109**, 246801 (2012).
[59] R. Nandkishore, J. Maciejko, D. A. Huse, and S. L. Sondhi, Phys. Rev. B **87**, 174511 (2013).
[60] M. S. Foster, H.-Y. Xie, and Y.-Z. Chou, Phys. Rev. B **89**, 155140 (2014).
[61] F. Zhang, A. H. MacDonald, and E. J. Mele, Proceedings of the National Academy of Sciences **110**, 10546 (2013).
[62] P. San-Jose and E. Prada, Phys. Rev. B **88**, 121408 (2013).
[63] S. Hattendorf, A. Georgi, M. Liebmann, and M. Morgenstern, Surface Science **610**, 53 (2013).
[64] J. S. Alden, A. W. Tsen, P. Y. Huang, R. Hovden, L. Brown, J. Park, D. A. Muller, and P. L. McEuen, Proceedings of the National Academy of Sciences **110**, 11256 (2013).
[65] L. Ju, Z. Shi, N. Nair, Y. Lv, C. Jin, J. Velasco Jr, C. Ojeda-Aristizabal, H. A. Bechtel, M. C. Martin,

A. Zettl, *et al.*, Nature **520**, 650 (2015).
[66] L.-J. Yin, H. Jiang, J.-B. Qiao, and L. He, Nature communications **7**, 11760 (2016).
[67] J. Li, K. Wang, K. J. McFaul, Z. Zern, Y. Ren, K. Watanabe, T. Taniguchi, Z. Qiao, and J. Zhu, Nature nanotechnology **11**, 1060 (2016).
[68] J. Li, R.-X. Zhang, Z. Yin, J. Zhang, K. Watanabe, T. Taniguchi, C. Liu, and J. Zhu, arXiv preprint arXiv:1708.02311 (2017).
[69] Q. Tong, H. Yu, Q. Zhu, Y. Wang, X. Xu, and W. Yao, Nature Physics **13**, 356 (2017).
[70] D. K. Efimkin and A. H. MacDonald, Phys. Rev. B **98**, 035404 (2018).
[71] S. Huang, K. Kim, D. K. Efimkin, T. Lovorn, T. Taniguchi, K. Watanabe, A. H. MacDonald, E. Tutuc, and B. J. LeRoy, Phys. Rev. Lett. **121**, 037702 (2018).
[72] X.-C. Wu, C.-M. Jian, and C. Xu, arXiv preprint arXiv:1811.08442 (2018).
[73] A. Altland and M. R. Zirnbauer, Phys. Rev. B **55**, 1142 (1997).
[74] C. L. Kane and M. P. A. Fisher, Phys. Rev. B **51**, 13449 (1995).